Received: 6 February 2024 | Revised: 2 July 2024 | Accepted: 28 July 2024

DOI: 10.1002/pro.5144

RESEARCH ARTICLE

THE PROTEIN SOCIETY WILEY

Structural basis for substrate flexibility of the *O*-methyltransferase MpaG′ involved in mycophenolic acid biosynthesis

Cai You[1,2,3] | **Yunjun Pan**[2] | **Ruxin Liu**[2] | **Shengying Li**[2,4] | **Yingang Feng**[1,3,5,6,7]

[1]CAS Key Laboratory of Biofuels, Shandong Provincial Key Laboratory of Synthetic Biology, Qingdao Institute of Bioenergy and Bioprocess Technology, Chinese Academy of Sciences, Qingdao, Shandong, China

[2]State Key Laboratory of Microbial Technology, Shandong University, Qingdao, Shandong, China

[3]Shandong Energy Institute, Qingdao, Shandong, China

[4]Laboratory for Marine Biology and Biotechnology, Qingdao Marine Science and Technology Center, Qingdao, Shandong, China

[5]Qingdao New Energy Shandong Laboratory, Qingdao, Shandong, China

[6]Shandong Engineering Laboratory of Single Cell Oil, Qingdao Institute of Bioenergy and Bioprocess Technology, Chinese Academy of Sciences, Qingdao, Shandong, China

[7]University of Chinese Academy of Sciences, Beijing, China

Correspondence
Shengying Li, State Key Laboratory of Microbial Technology, Shandong University, Qingdao, Shandong 266237, China.
Email: lishengying@sdu.edu.cn

Yingang Feng, CAS Key Laboratory of Biofuels, Shandong Provincial Key Laboratory of Synthetic Biology, Qingdao Institute of Bioenergy and Bioprocess Technology, Chinese Academy of Sciences, Qingdao, Shandong 266101, China.
Email: fengyg@qibebt.ac.cn

Funding information
National Key Research and Development Program of China, Grant/Award Number: 2023YFC3402300; National Natural Science Foundation of China, Grant/Award Numbers: 22237004, 32200030, 32070125; State Key Laboratory of Microbial Technology Open Projects Fund, Grant/Award Number: M2022-01; QIBEBT, Grant/Award Number: QIBEBT/SEI/QNESL S202302; China National Postdoctoral Program for Innovative Talents, Grant/Award Number: BX20240210; China Postdoctoral Science

Abstract

MpaG′ is an *S*-adenosyl-L-methionine (SAM)-dependent methyltransferase involved in the compartmentalized biosynthesis of mycophenolic acid (MPA), a first-line immunosuppressive drug for organ transplantations and autoimmune diseases. MpaG′ catalyzes the 5-*O*-methylation of three precursors in MPA biosynthesis including demethylmycophenolic acid (DMMPA), 4-farnesyl-3,5-dihydroxy-6-methylphthalide (FDHMP), and an intermediate containing three fewer carbon atoms compared to FDHMP (FDHMP-3C) with different catalytic efficiencies. Here, we report the crystal structures of *S*-adenosyl-L-homocysteine (SAH)/DMMPA-bound MpaG′, SAH/FDHMP-3C-bound MpaG′, and SAH/FDHMP-bound MpaG′ to understand the catalytic mechanism of MpaG′ and structural basis for its substrate flexibility. Structural and biochemical analyses reveal that MpaG′ utilizes the catalytic dyad H306-E362 to deprotonate the C5 hydroxyl group of the substrates for the following methylation. The three substrates with differently modified farnesyl moieties are well accommodated in a large semi-open substrate binding pocket with the orientation of their phthalide moiety almost identical. Based on the structure-directed mutagenesis, a single mutant MpaG′$_{Q267A}$ is engineered with significantly improved catalytic efficiency for all three substrates. This study expands the mechanistic understanding and the pocket engineering strategy for *O*-methyltransferases involved in fungal natural product biosynthesis.

Cai You and Yunjun Pan have contributed equally to this study.

Foundation, Grant/Award Number: 2023M742087

Review Editor: John Kuriyan.

Our research also highlights the potential of *O*-methyltransferases to modify diverse substrates by protein design and engineering.

KEYWORDS

crystal structure, mycophenolic acid, *O*-methyltransferase, protein engineering, substrate flexibility

1 | INTRODUCTION

Mycophenolic acid (MPA), the first natural product antibiotic to be isolated and crystallized, was discovered from a strain of *Penicillium brevicompactum* in 1893 (Bentley, 2000; You et al., 2021; Zhang et al., 2019). As the first-line immunosuppressant, MPA is widely utilized in organ transplantations and the treatment of autoimmune diseases due to its excellent antiviral (Planterose, 1969) and immunosuppressive activities (Mitsui & Suzuki, 1969). In addition, continuous studies have revealed its antimicrobial, anticancer, antithrombotic, and other considerable activities, making it a prominent candidate for drug development and medical applications (Kourounakis et al., 2020; Vaishnav & Demain, 2011).

Previously, we identified the MPA biosynthetic gene cluster (BGC) (Zhang et al., 2015) and fully elucidated the biosynthetic pathway in *Penicillium brevicompactum* NRRL 864 (Pb_{864}), which features a unique interplay between secondary metabolism (the BGC-based assembly of the meroterpenoid core structure) and primary metabolism (the post-tailoring of the farnesyl side chain by peroxisomal β-oxidation machinery), along with an intricate biosynthetic process mediated by highly compartmentalized enzymes (Figure S1) (Du & Li, 2021; Zhang et al., 2019). In this biosynthetic pathway, the cytosolic *S*-adenosyl-L-methionine (SAM)-dependent *O*-methyl transferase MpaG′ is capable of accepting multiple intermediates as substrates during the biosynthetic and β-oxidation processes. In addition to catalyzing the 5-*O*-methylation of demethylmycophenolic acid (DMMPA) to form MPA, MpaG′ can also methylate the earlier intermediates 4-farnesyl-3,5-dihydroxy-6-methylphthalide (FDHMP) and FDHMP-3C (an intermediate containing three fewer carbon atoms compared to FDHMP), thereby diversifying the MPA biosynthetic pathway (Du & Li, 2021; You et al., 2021; Zhang et al., 2019) (Figure 1). All these substrates share an identical phthalide moiety (the head) containing the site to be methylated, but they have the differently modified farnesyl side chain (the tail).

Methyltransferases are vital enzymes ubiquitously distributed in plants, animals, and microorganisms (Liscombe et al., 2012). Most methyltransferases use the co-substrate SAM as an electron-deficient methyl donor, which transfers a methyl group to a nucleophilic atom via an S_N2 mechanism (Lin et al., 2023). Some methyltransferases can facilitate the methylation of complex compounds by generating reactive free radicals through the homolytic cleavage of SAM. These methyltransferases are classified as radical SAM enzymes and play crucial roles in the biosynthesis of many natural products (Knox et al., 2022; Lee et al., 2023). Methyltransferases can

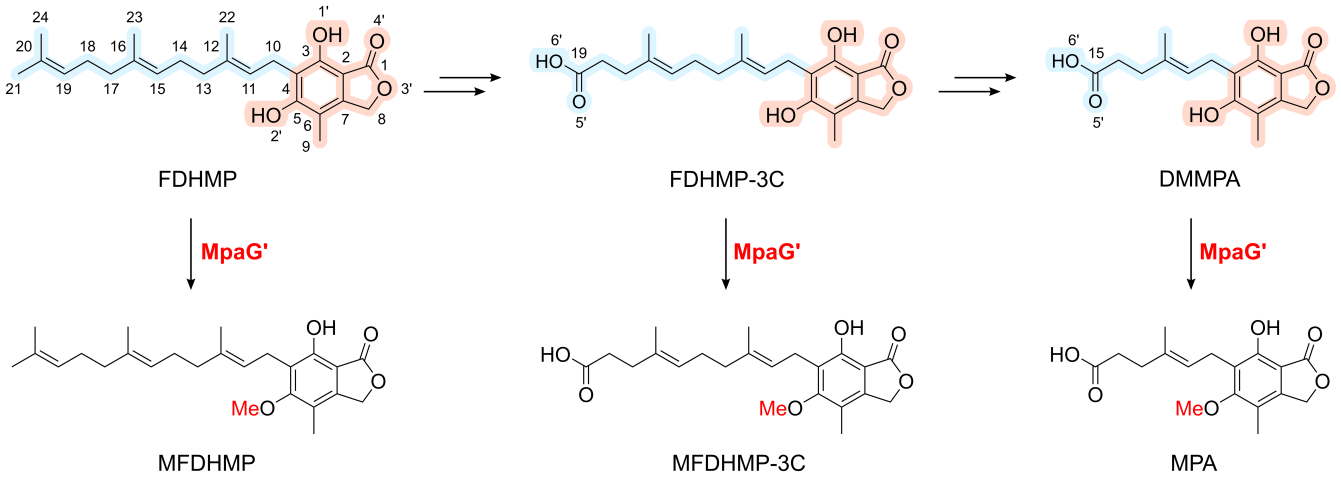

FIGURE 1 The biosynthetic steps mediated by the *O*-methyltransferase MpaG′. The methyl groups installed by MpaG′ are marked in red. The heads and tails of substrates are shaded in orange and blue, respectively.

catalyze DNA methylation, playing significant regulatory roles in gene expression as well as in the growth and development of organisms (Subrizi et al., 2021; Yang et al., 2006). Moreover, methyltransferases mediate the methylation of various metabolites in diverse physiological processes, thereby participating in both synthesis and breakdown of biologically active substances (Zhang & Zheng, 2016). Normally, methyltransferases are categorized into *O*- (Zhang et al., 2015; Zhang et al., 2019), *S*- (Scharf et al., 2014), *C*- (Li et al., 2021), and *N*-methyltransferases (Scharf et al., 2014), and other acceptor-directed methyltransferases (Li et al., 2021; Lin et al., 2023), according to the specific atom to be methylated in the methyl-accepting substrates. Among them, *O*-methyltransferases account for ~54% of total methyltransferases and hold great biological significance (Lin et al., 2023).

In our previous study, we conducted in vitro biochemical analysis on MpaG′ and revealed the remarkable substrate flexibility of this *O*-methyltransferase (Zhang et al., 2015; Zhang et al., 2019). However, the lack of structural information for MpaG′ makes it challenging to understand its catalytic mechanism and the molecular basis underlying its broad substrate specificity. Thus, herein, we resolved the crystal structures of *S*-adenosyl-L-homocysteine (SAH)/DMMPA-bound MpaG′, SAH/FDHMP-3C-bound MpaG′ and SAH/FDHMP-bound MpaG′. We analyzed the structures and provided a mechanistic understanding of the catalysis and substrate flexibility, combining the mutagenesis and biochemical analyses. We also developed an effective strategy for semi-rational engineering of MpaG′ to enhance the MPA production, and highlighted the potential of protein design and engineering for *O*-methyltransferases towards diverse substrates.

2 | MATERIALS AND METHODS

2.1 | Gene cloning

The DNA sequence encoding MpaG′ was amplified by standard PCR method using *Penicillium brevicompactum* NRRL 864 (Pb_{864}) cDNA as a template. The PCR fragment was inserted into the expression vector pETM11 (EMBL) using *Nco*I and *Xho*I restriction sites. All the recombinant proteins were expressed to contain an *N*-terminal His_6-tag and a tobacco etch virus (TEV) protease cleavage site.

2.2 | Site-directed mutagenesis

The expression vector pETM11-MpaG′ was used for the expression of wild-type MpaG′. The mutants were constructed by site-directed mutagenesis via overlap extension PCR using the specific mutagenesis primers as listed in Table S1. All constructed plasmids were verified by DNA sequencing.

2.3 | Strains

The whole genome of wild-type Pb_{864} was previously sequenced and assembled (Zhang et al., 2015). To delete *mpaG′*, the upstream and downstream sequences of *mpaG′* were PCR-amplified from the genomic DNA of Pb_{864} by the primer pairs *mpaG′*d-UF/*mpaG′*d-UR and *mpaG′*d-DF/*mpaG′*d-DR, respectively. Subsequently, the amplified sequences were fused with the hygromycin resistance gene cassette (*hph*) (Cullen et al., 1987), serving as a selection marker, by using the double-joint PCR method (Pan et al., 2020; Yu et al., 2004). This process allowed us to generate the deletion cassette for *mpaG′*, and the *mpaG′* gene was replaced by this cassette in Pb_{864} via homologous recombination. All the primers are listed in Table S2.

2.4 | Preparation of substrates

The substrate DMMPA was prepared using the *mpaG′* knockout strain Pb_{864}-Δ*mpaG′*. Specifically, this knockout strain was cultured on the surface of potato dextrose agar to obtain conidia. The fresh conidia were inoculated into 100 ml PDB medium in a 300 ml conical flask, which was grown at 30°C and 150 rpm for 6 days. Afterward, the mycelia-containing fermentation broth was extracted by ethyl acetate twice, followed by purification using semi-preparative C18 reverse-phase HPLC. The substrates FDHMP-3C and FDHMP were obtained from the fermentation extract of the recombinant strain $Ao_{M\text{-}2\text{-}3}$-*mpaA′*-*mpaB′* (Zhang et al., 2019). The strain was cultivated in DPY medium enriched with maltose to induce the co-expression of MpaA′ and MpaB′ for 3 days, followed by the addition of 3,5-dihydroxy-6-methylphthalide (DHMP) to a final concentration of 0.56 mM. After an additional 6-d cultivation, the fermentation broth was extracted twice with 2-time volumes of ethyl acetate. The organic extracts were then concentrated and dried using a rotary evaporator before being re-dissolved in methanol. Finally, all substrates were isolated and purified by semi-preparative HPLC.

2.5 | Protein expression and purification

The sequence-verified constructs were transformed into *Escherichia coli* BL21(DE3) for recombinant protein

overexpression. The bacteria were cultured in Luria-Bertani (LB) medium at 37°C until the value of OD_{600} reached ~0.6, and then 0.2 mM IPTG was added to induce protein expression, with further culturing at 16°C overnight. Cells were harvested and disrupted by sonication in lysis buffer containing 50 mM Tris–HCl, 500 mM NaCl, 20 mM β-mercaptoethanol, 10% glycerol, 1% Tween-80, pH 8.0. The lysates were centrifugated (14,000*g*, 40 min) at 4°C and the supernatant was loaded onto a nickel-chelating Sepharose affinity chromatography column (GE Healthcare), and the column was washed with 10-bed volumes of wash buffer (lysis buffer plus 20 mM imidazole). The His_6-tagged protein was eluted with elution buffer (50 mM Tris–HCl, 500 mM NaCl, 20 mM β-mercaptoethanol, 300 mM imidazole, 10% glycerol, pH 8.0) and exchanged to the buffer containing 50 mM Tris–HCl, 500 mM NaCl, pH 8.0 with PD-10 Desalting Columns for His_6-tag removal by TEV protease. Further purification was performed by size-exclusion chromatography using a HiLoad 16/60 Superdex 200 column (GE Healthcare) in the buffer containing 25 mM HEPES, 150 mM NaCl, pH 7.5. The purified proteins were concentrated to approximately 8–15 mg/ml as determined by absorbance at 280 nm and stored in aliquots at −80°C after flash freezing in liquid nitrogen. The purification method for the mutants was the same as that for the wild-type MpaG′. The purity of purified proteins was checked by polyacrylamide gel electrophoresis (Figure S2).

2.6 | In vitro enzymatic assay of MpaG'

The analytical scale reaction containing 1 μM MpaG′ (wild type or mutant), 5 mM SAM and 0.5 mM substrate in 100 μl storage buffer (50 mM NaH_2PO_4, 10% glycerol, pH 8.0) was incubated at 40°C (the maximum activity of MpaG′ was observed at 40°C) (Zhang et al., 2015) for 1 h, which was quenched by adding an equal volume of methanol. The mixture was subjected to high-speed centrifugation (12,000*g*, 15 min) to remove precipitated proteins before analyzing the reaction by HPLC. Control experiments were conducted to ensure no significant product inhibition by SAH under the assay conditions (Muth & Nash, 1975).

2.7 | Crystallization and structure determination

The crystallization experiments were performed with the sitting-drop vapor-diffusion method at 18°C. The drops contained an equal volume of protein sample and reservoir solution. Before crystal screening, MpaG′ was incubated with DMMPA and SAH or FDHMP-3C and SAH or FDHMP and SAH at a molar ratio of 1:10:5 for 1 h at 4°C. After optimization, the best crystals of MpaG′/DMMPA/SAH complexes were grown in drops containing 15% PEG3350 (*w*/*v*), 0.1 M sodium cacodylate, pH 6.0 and 0.2 M magnesium chloride. Crystals of MpaG′/FDHMP-3C/SAH complexes were grown with a reservoir solution containing 10% PEG 8000 (*w*/*v*), 0.1 M CHES, pH 9.5, and 0.2 M sodium chloride. Crystals of MpaG′/FDHMP/SAH complexes were grown in drops containing 15% PEG3350, 0.1 M sodium cacodylate, pH 6.0, and 0.2 M sodium chloride. The crystallization solution added with 20% glycerol served as the cryoprotectant for all the crystals. Suitable crystals were quickly soaked in the cryo-protectant solution and frozen directly in liquid nitrogen.

The diffraction data were collected on the BL19U1 and BL02U1 beamlines at the Shanghai Synchrotron Radiation Facility (SSRF) (Wang et al., 2018; Zhang et al., 2019). The data were processed by XDS (Kabsch, 2010). Structures of MpaG′/DMMPA/SAH, MpaG′/FDHMP/SAH, and MpaG′/FDHMP-3C/SAH complexes were all solved by molecular replacement with MpaG′ model structure (Figure S3) constructed by AlphaFold2 (Jumper et al., 2021) as the search model using Phaser (McCoy et al., 2007). All the structures were refined with PHENIX (Adams et al., 2010) and COOT (Emsley et al., 2010). All the final models were evaluated using MolProbity (Williams et al., 2018). The statistics of all the crystallographic data and final refined structures are summarized in Table S3. All protein structure graphics were created with PyMOL (http://www.pymol.org).

2.8 | Steady-state kinetics

The reactions of MpaG′ were carried out with a volume of 145 μl in 1.5 ml centrifugation tubes. The reaction containing MpaG' (30–500 nM) and substrate (10–500 μM) in 145 μl storage buffer (50 mM NaH_2PO_4, 10% (*w*/*v*) glycerol, pH 8.0) was incubated at 40°C for 2 min. Then, the reactions with different substrate concentrations were initiated by adding SAM (5 μl) to the final concentration of 500 μM, and three aliquots (50 μl) were taken at three time points (0, 0.5, and 1 min for the reactions with substrate concentrations <50 μM; 0, 1.5, and 2 min for the reactions with substrate concentrations >100 μM) within the linear range. These aliquots were individually mixed thoroughly with 50 μl of methanol to terminate the reactions. Proteins were removed by centrifugation at 15,000*g* for 10 min. The supernatant was subject to HPLC analysis to monitor substrate consumption within the linear range, thereby allowing calculation of the initial velocity

of *O*-methylation reactions. The analytic HPLC conditions were as follows: reversed-phase HPLC column (C18, 5 μm, 150 mm, Agilent 1220), solvent B (acetonitrile + 0.1% TFA; DMMPA: 40%–60%, FDHMP-3C: 55%–75%, FDHMP: 80%–100%) in solvent A (deionized H_2O + 0.1% TFA) over 20 min, flow rate 1.0 ml min^{-1}, UV wavelength 254 nm. All measurements were conducted in duplicate, and the velocities determined at various substrate concentrations were fit to the Michaelis–Menten equation to calculate the steady-state kinetic parameters.

3 | RESULTS

3.1 | Preparation of MpaG′ substrates

To obtain the substrates of MpaG′, we constructed a *mpaG′* deletion mutant of Pb_{864} (*Pb*-Δ*mpaG′*) via homologous recombination. As expected, *Pb*-Δ*mpaG′* completely lost its ability to synthesize MPA and accumulated a significant amount of DMMPA (Figure S4). However, FDHMP-3C and FDHMP, which are also substrates of MpaG′, were not produced by *Pb*-Δ*mpaG′* due to the downstream transformations. To prepare these two intermediates, the recombinant strain of *Aspergillus oryzae* M-2-3 ($Ao_{M\text{-}2\text{-}3}$) containing a plasmid for heterologous co-expression of MpaA′ and MpaB′ (i.e., $Ao_{M\text{-}2\text{-}3}$-*mpaA′-mpaB′*) was used because this strain was proved to produce FDHMP-3C and FDHMP in our previous study (Zhang et al., 2019). Sufficient amounts of DMMPA, FDHMP-3C, and FDHMP were finally obtained with high purity for the preparation of the MpaG′-substrate complexes and biochemical assays.

3.2 | The structure of the MpaG′/SAH/DMMPA complex

To elucidate the structural basis of the methylation activity and substrate specificity of MpaG′ (Figure S5), we first determined the structure of MpaG′ in complex with SAH (the demethylated product of SAM to mimic the structure of reactive SAM) and DMMPA at 2.0 Å resolution in space group $P3_2$. The complex structure was solved using the molecular replacement method, with six molecules in one asymmetric unit forming three dimers.

The sequence and structure characteristics of MpaG′ classify it as a class I methyltransferase, which typically exhibits the features of Rossmann fold (Liscombe et al., 2012; Schubert et al., 2003) (Figure S6). The *N*-terminal domain (residues 1–129), mainly composed of α-helices, is responsible for the dimerization of MpaG′ (Figure 2a). Two monomers intertwine through this part and make a large dimer interface, with the accessible surface area (ASA) buried in the interface amounting to 4515 $Å^2$ as calculated by PDBePISA (Krissinel & Henrick, 2007). It is noteworthy that a four-helix bundle composed of a pair of *N*-terminal helices (α1 and α2 from one monomer and α1′ and α2′ from the other monomer) contribute largely to the buried surface area in the dimer (Figure 2b). The *C*-terminal catalytic domain (residues 130–398) consists of two subdomains: one helical subdomain containing five helices including α8, α9, α10, α11 and α16, and a classical α/β Rossmann fold subdomain with a seven-stranded β-sheet in the core surrounded by five helices (α12, α13, α14, α15 and α17) (Figure 2a). The substrate binding cavity is formed between the two subdomains. The SAM mimic SAH binding site is located at the Rossmann fold subdomain, while the binding site of the methyl receptor is located at the helical subdomain. Besides, an *N*-terminal helix α3′ from the other monomer also participates in the formation of the methyl receptor binding site (Figure 2b). With clear electron densities, SAH and the methyl receptor DMMPA are well defined within the catalytic domain (Figures 2c and S7a), which enables us to analyze the details of the substrate binding mode.

The SAH molecule makes extensive interactions with the Rossmann fold subdomain, especially the conserved DXGXGXG motif (Joshi & Chiang, 1998) (^{237}DVGGGRG^{243} in MpaG′) (Figures 2c and S8a). The adenosine ring is anchored by I287 and D286 via hydrogen bonds. The O3′ and O2′ atoms of the ribose moiety form a pair of hydrogen bonds with the Oδ1 and Oδ2 atoms of D264. The tail of SAH is tightly fixed by the main chain and side chain atoms of M200, Y203, G239, H244, and H302 via extensive hydrogen bonds and potential salt bridges formed between the tail carboxyl group and the side chains of H244 and H302 (Figures 2c and S8a).

The substrate DMMPA is located in a substrate binding site adjacent to SAH (Figure 2d). DMMPA interacts extensively with the helices α10, α11 and α16 of the helical subdomain, and the loop between α15 and β6 of the Rossmann fold subdomain (Figure 2a). In addition, DMMPA interacts with W54 from α3′ of the other monomer via hydrophobic and possible π–π interactions (Figure 2d), suggesting that the dimerization may contribute to substrate binding and perhaps enzymatic activity as well. Overall, DMMPA is well accommodated in the semi-open pocket which is predominantly hydrophobic owing to residues W54, F182, L186, F196, M200, Y203, V304, F308, I353, M354, and M358 (Figures 2d and S8a). The head part, especially the phthalide moiety is buried deeply in the pocket. It is anchored by F196 via π–π stacking and H357 via lone pair-π stacking (Figures 2d and S8a). Among these interactions, the π–π

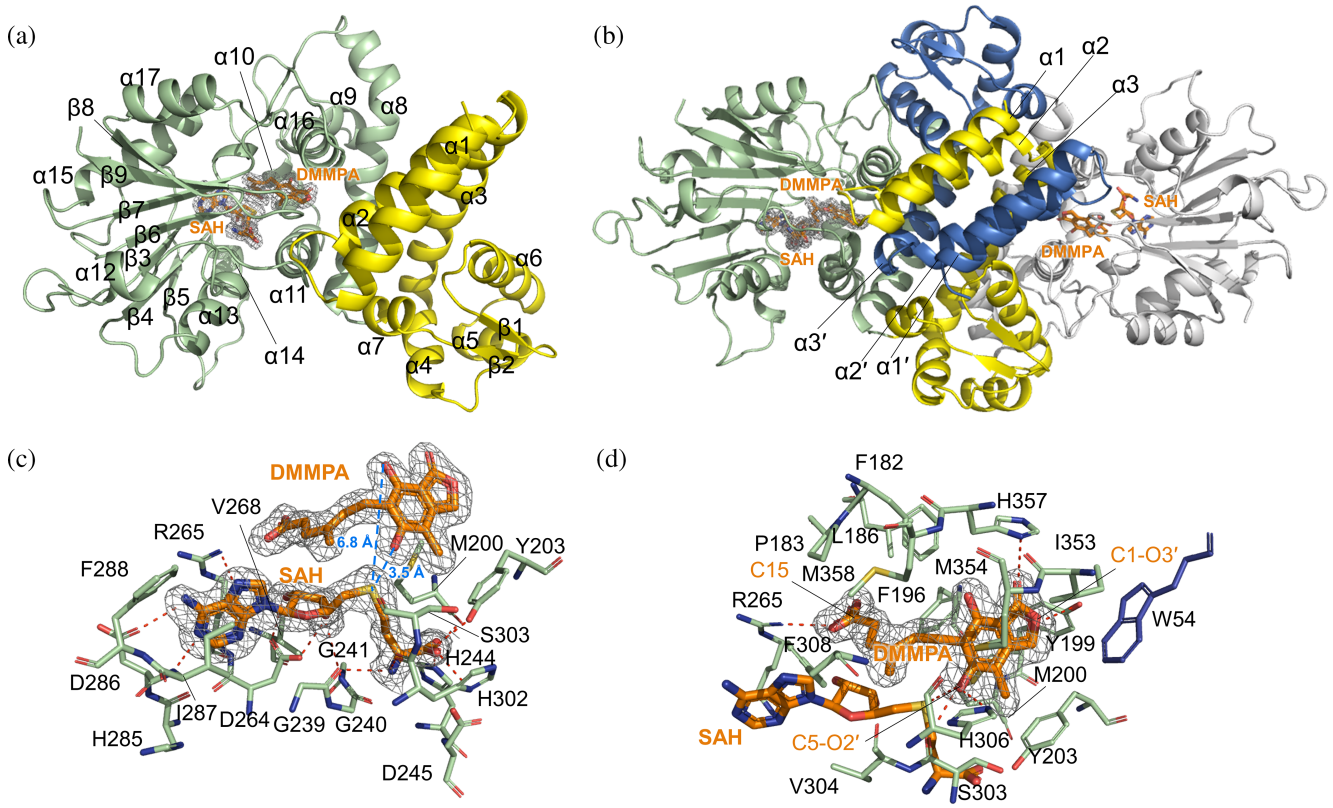

FIGURE 2 Structural analysis of MpaG′/SAH/DMMPA complex. (a) Cartoon representation of the overall structure of MpaG′. The *N*-terminal dimerization domain and *C*-terminal catalytic domain are colored in yellow and pale green, respectively. The SAH and DMMPA molecules are both colored orange and shown as stick representations with a gray mesh illustrating the $2mF_o$–DF_c electron density map contours at the 1.0 σ level. (b) The dimeric state of MpaG′. One protomer is colored as presented in (a), and for the other protomer, the *N*-terminal and *C*-terminal domains are colored in blue and gray, respectively. (c) The enlarged view of the SAH binding pocket. The SAH and DMMPA molecules are presented as orange sticks. Hydrogen bonds and salt bridges are represented as red dashed lines. The distances between the sulfonium of SAH and the O1′/O2′ of DMMPA are indicated by blue dashed lines. (d) The enlarged view of the DMMPA binding pocket, with hydrogen bond and salt bridge interactions indicated by red dashed lines.

interaction mediated by F196 is believed to have a pivotal role in the enzymatic activity towards DMMPA. To test this hypothesis, we disrupted this interaction by generating a mutant MpaG′$_{F196A}$, and found that this mutation completely abolished the methylation activity (Figure 3a). We reason that the π–π stacking facilitated by F196 is likely responsible for orienting the substrate head and preserving its proper conformation within the substrate binding pocket.

In addition, residue Y199 hydrogen bonds to the C1-O3′ atom of DMMPA, and the C5-O2′ atom accepts a pair of hydrogen bonds from S303 and H306 (Figures 2d and S8a). The C15 carboxyl group forms a salt bridge with R265, thereby facilitating the tail of DMMPA in the right orientation (Figures 2d and S8a). We surmised that the role of R265 in anchoring the substrate's tail via a salt bridge might be as important as the above-described function of F196 in stabilizing the substrate's head. However, compared with the activity of MpaG′$_{WT}$ towards DMMPA (67.9 ± 2.7% conversion), MpaG′$_{R265A}$ only exhibited a 0.39-fold decreased activity (41.7 ± 1.7% conversion) (Figure 3a). These results indicate that the substrate's head is more important than the substrate's tail in productive substrate binding process.

The class I SAM-dependent *O*-methyltransferases have been reported to use acid/base activation for catalysis by a highly conserved Glu/His dyad (Liao et al., 2020; Newmister et al., 2018; Zubieta et al., 2001). Through sequence alignment with homologous proteins and concomitant structural analysis, the catalytic dyad of MpaG′ was identified as H306-E362 (Figures S6 and S9). The essential roles of these two catalytic residues were confirmed by mutating each residue to alanine. As expected, towards the three substrates, the purified MpaG′$_{E362A}$ showed a significant decrease in methylation activity, and MpaG′$_{H306A}$ completely lost the methyltransferase activity (Figure 3). In the catalytic process, the general base H306 is likely activated by E362 to deprotonate the

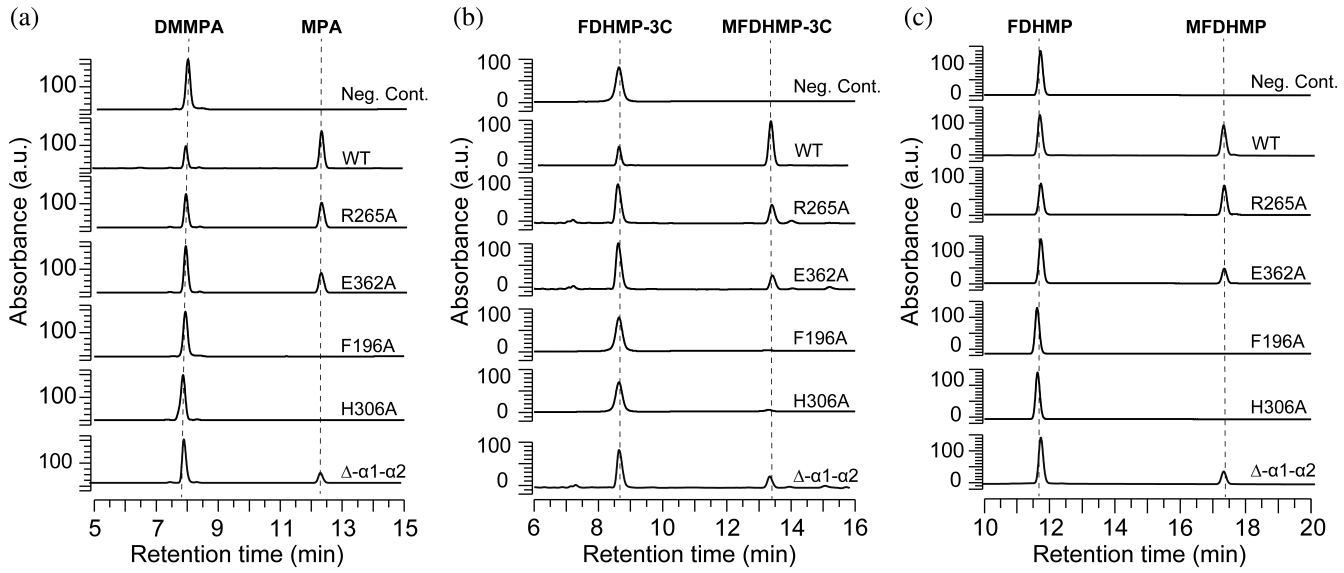

FIGURE 3 HPLC analysis (254 nm) of the enzymatic reactions catalyzed by the wild type (WT) and mutant MpaG′ enzymes using DMMPA (a), FDHMP-3C (b), and FDHMP (c) as substrates. The analytical scale reactions containing 1 μM MpaG′ (wild type or mutant), 5 mM SAM, and 0.5 mM substrate in 100 μl storage buffer were incubated at 40°C for 1 h.

C5 hydroxyl group of substrates (Figure S9). Supporting this, the C5 hydroxyl group is positioned within the hydrogen bonding distance with H306. The non-reactive product SAH lacking the sulfonium methyl group of SAM is oriented to the O2′ of the C5 hydroxyl group with a distance to the sulfonium moiety of 3.5 Å (Figure 2c). The head part of DMMPA is fixed in the structure by various interactions (Figures 2d and S8a), resulting in a 6.8 Å distance between the sulfonium moiety and the O1′ of the C3 hydroxyl group (Figure 2c). This position of SAH is speculated to mimic the actual conformation of SAM in the methylation reaction, in agreement with the regioselectivity of MpaG′.

3.3 | The structure of MpaG′/SAH/FDHMP-3C complex

To explore the mechanism for substrate diversity of MpaG′, we further determined the structure of MpaG′/SAH in complex with FDHMP-3C at 2.13 Å resolution in space group $H3_2$. According to the electron densities, SAH and the methyl receptor FDHMP-3C are well present in the active site (Figures 4a and S7b). Superimposing the MpaG′/SAH/FDHMP-3C complex onto the MpaG′/SAH/DMMPA complex reveals very similar conformation with a root-mean-square deviation (RMSD) of 0.17 Å for the aligned Cα atoms (Figure 4b).

The binding mode of SAH is almost identical to that in MpaG′/SAH/DMMPA complex, mainly through hydrogen bonds, salt bridges, and hydrophobic interactions (Figures 4c and S8b). Benefiting from the semi-open substrate pocket, FDHMP-3C with a longer tail than DMMPA is also well accommodated in the substrate binding site in a manner similar to DMMPA (Figures 4d, e and S8b). Again, the binding pocket is largely hydrophobic with the phthalide moiety buried in deep. Three residues Y199, S303, and H306 interact with the phthalide moiety of FDHMP-3C via hydrogen bonds, and residues H357 and F196 contribute lone pair-π stacking and π–π stacking, respectively. The key role of F196 in coordinating FDHMP-3C was confirmed by an in vitro enzymatic assay, showing that the mutant MpaG′$_{F196A}$ completely lost the activity towards FDHMP-3C (Figure 3b). The identical interactions for DMMPA and FDHMP-3C support the same regioselectivity of MpaG′ on both substrates. The positions of the residues contributing to the hydrophobic interactions are almost the same as those in the DMMPA binding pose (Figures 4c and S8a,b). Nevertheless, the longer tail of FDHMP-3C inevitably causes some conformational changes (Figure 4e). Specifically, the side chain of R265 swings closely to the carboxyl group of FDHMP-3C to form a salt bridge with the C19-O5′ atom. Besides, a new residue Q267, nonparticipating in the interaction with DMMPA, is oriented to hydrogen bond to the C19-O6′ atom of the carboxyl group with a distance of 2.7 Å (Figures 4e and S8b).

With these observations, we examined the contribution of R265 in anchoring the tail of FDHMP-3C. Similar to that observed in DMMPA, MpaG′$_{R265A}$ exhibited impaired enzymatic activity towards FDHMP-3C, with only 35.6 ± 2.7% activity retained compared with MpaG′$_{WT}$ (76.6 ± 0.3% conversion) (Figure 3b).

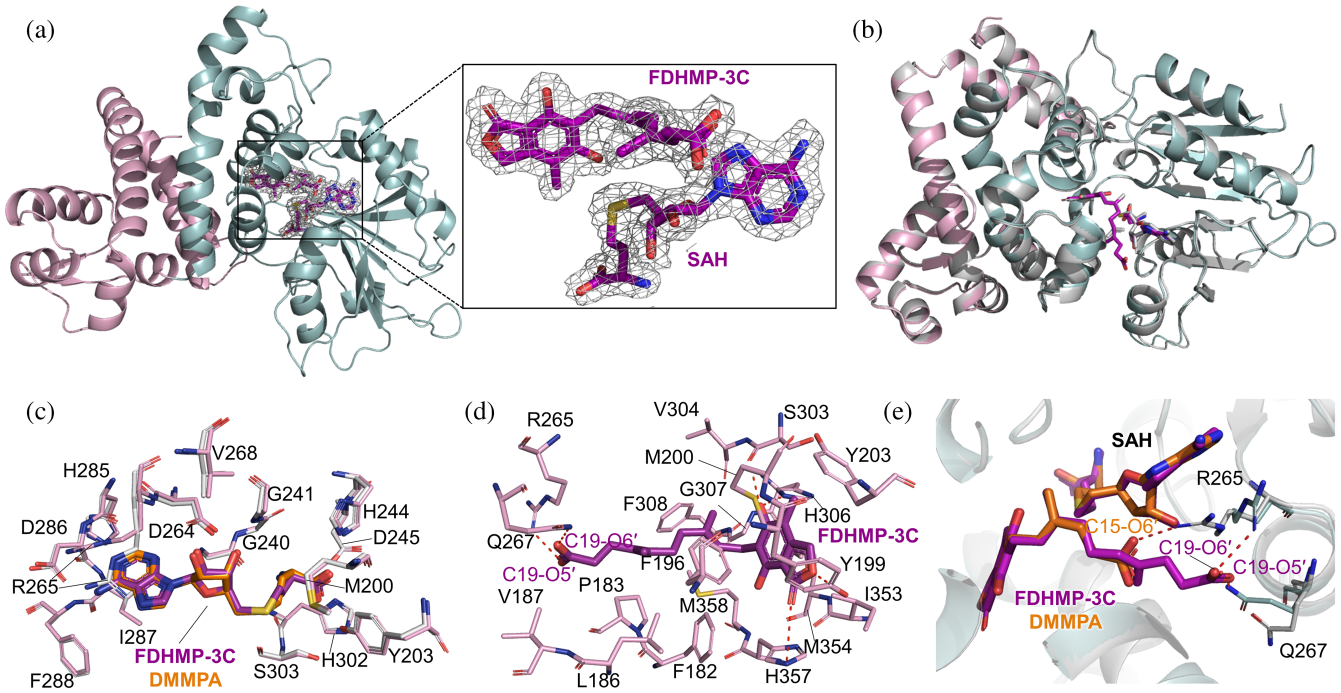

FIGURE 4 Structural analysis of MpaG′/SAH/FDHMP-3C complex. (a) The overall structure of the MpaG′/SAH/FDHMP-3C complex. The *N*-terminal and *C*-terminal catalytic domains are colored pink and pale cyan, respectively. The enlarged view of SAH and FDHMP-3C is shown as purple sticks with a gray mesh illustrating the $2mF_o$–DF_c electron density map contours at the 1.0 σ level. (b) Superimposition of the MpaG′/SAH/FDHMP-3C complex and the MpaG′/SAH/DMMPA complex (gray). (c) Structural comparison of SAH binding pockets from MpaG′/SAH/FDHMP-3C (SAH, purple; residues, pink) and MpaG′/SAH/DMMPA (SAH, orange; residues, gray). (d) The enlarged view of the FDHMP-3C binding pocket, with hydrogen bond and salt bridge interactions indicated by red dashed lines. (e) Alternative conformations of the two residues R265 and Q267 in MpaG′/SAH/FDHMP-3C (SAH, FDHMP-3C, purple; residues, pale cyan) and MpaG′/SAH/DMMPA (SAH, DMMPA, orange; residues, gray).

3.4 | The crystal structure of MpaG′/SAH/FDHMP complex

FDHMP is a substrate with a longer side chain than FDHMP-3C and the tail is completely hydrophobic. This molecule can also be methylated by MpaG′. To elucidate the substrate recognition mechanism of MpaG′ on FDHMP, we further determined the crystal structure of the MpaG′/SAH/FDHMP ternary complex at 1.99 Å resolution in space group $P3_2$. Six molecules form three dimers in one asymmetric unit, and the well-modeled chain A was selected for subsequent analysis. The MpaG′/SAH/FDHMP complex displays a nearly identical overall fold to those of the MpaG′/SAH/DMMPA complex and MpaG′/SAH/FDHMP-3C complex, with RMSD values of 0.13 Å and 0.18 Å, respectively, for the aligned Cα atoms.

In the complex, the cofactor SAH and substrate FDHMP are well accommodated within their binding pocket as determined by strong electron densities (Figures 5a and S7c). This pocket is predominantly hydrophobic owing to many bulky hydrophobic residues (Figures 5a and S8c). In addition, the phthalide moiety of FDHMP is anchored by residues F196, H306 and H357 through π-stacking and hydrogen bonds. Among them, F196 plays a pivotal role in fixing the orientation of FDHMP, as confirmed by the enzymatic activity assay (Figure 3c). This finding is consistent with the results obtained for the two alternative substrates as described above. However, the salt bridge between R265 and FDHMP is unavailable as that for DMMPA or FDHMP-3C due to its completely hydrophobic tail (Figures 5a and S8). Consistent with this, the catalytic activities of MpaG′$_{R265A}$ (42.7 ± 3.8% conversion) and MpaG′$_{WT}$ (43.2 ± 4.9% conversion) were comparable in enzyme activity assays when using FDHMP as substrate (Figure 3c). The structural alignment of these complex structures suggests that the orientation of the phthalide moiety in the three substrates is nearly identical, consistent with the identical regioselectivity for these substrates. Moreover, the orientations of the side chains of these substrates are remarkably similar (Figure 5b). The proper orientation of the phthalide moiety ensures that the C5 hydroxyl group is within the reacting distance to the catalytic base H306. Even with the longest chain, FDHMP is well positioned in an extended conformation in the substrate binding

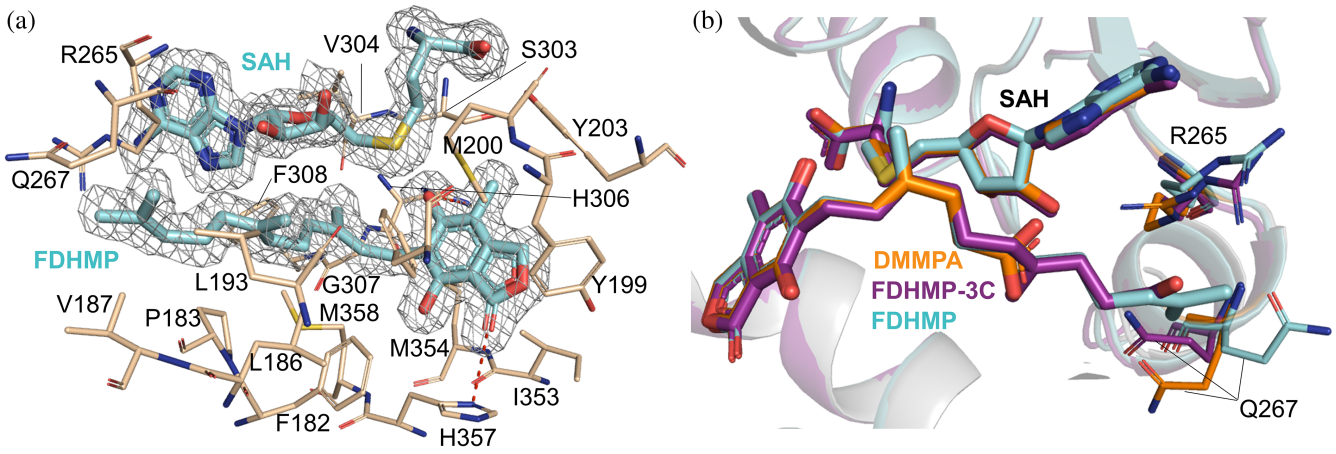

FIGURE 5 Analysis of the MpaG′/SAH/FDHMP complex structure. (a) The binding pocket of FDHMP. The SAH and DMMPA molecules are shown in cyan sticks with a gray mesh illustrating the $2mF_o$–DF_c electron density map contours at the 1.0 σ level. Residues interacting with FDHMP are displayed as wheat sticks. Hydrogen bonds are represented as red dashed lines. (b) Structural alignment of three substrates DMMPA (orange), FDHMP-3C (purple), and FDHMP (cyan) in the complex structures.

pocket. Its hydrophobic tail is fully coordinated by multiple residues (P183, L186, V187, L193, R265, and Q267) through hydrophobic interactions (Figures 5a and S8c). In the enzyme-substrate complexes, three different substrates are all accommodated in a common hydrophobic binding pocket formed by similar hydrophobic residues (Figure S8). It is worth noting that the conformations of R265 and Q267 undergo significant changes to match the distinct tail structures (Figure 5b). In the complex structure of MpaG′/SAH/FDHMP, the polar side chains of both R265 and Q267 are positioned away from the hydrophobic tail of FDHMP (Figure 5b).

3.5 | The steady-state kinetic parameters of MpaG′

As observed in the three solved complex structures, each substrate (DMMPA, FDHMP-3C, or FDHMP) can all be well accommodated within the substrate binding pocket. To quantitatively assess the catalytic efficiencies of MpaG′ for these three substrates, steady-state kinetic analyses were performed by measuring the initial substrate consumption rates with high-performance liquid chromatography (HPLC). As a result, MpaG′ exhibited similar k_{cat} values towards the three substrates (Table 1 and Figure S10a). This finding is consistent with the structural analyses (Figures 2, 4, and 5), as the phthalide-moieties of the three substrates that are involved in the methyl-transferring process adopt nearly identical conformations within the deep binding pocket. With regard to substrate binding affinities, the K_m value of FDHMP-3C to MpaG′ was determined to be 2.7 and 3.9 times lower than those of DMMPA and FDHMP to MpaG′, respectively. It is evident that FDHMP-3C and FDHMP with the k_{cat}/K_m values of 2.7 and 0.7 min^{-1} μM^{-1} are the most favorable and unfavorable substrates of MpaG′, respectively, among the three substrates, which are well-consistent with the substrate conversion results (Figure 3). Structurally, FDHMP-3C, which possesses a longer tail than DMMPA, has more extensive interactions with the binding pocket residues compared to DMMPA. By contrast, the longer and more hydrophobic tail (due to the lack of the terminal carboxyl group) of FDHMP is less favorable than the polar, negatively charged tail of FDHMP-3C for its proper positioning in the pocket.

3.6 | Comparison with other methyltransferases

By submitting the MpaG′ complex structures to the Dali server (Holm & Rosenström, 2010), we identified a number of structure homologs. The closest homolog turned out to be a SAM-dependent *O*-methyltransferase-like pericyclase LepI (PDB code: 6IX7), which catalyzes pericyclic reactions in leporin biosynthesis (Cai et al., 2019; Liao et al., 2020; Sun et al., 2019), with an RMSD of 2.2 Å for the aligned Cα atoms. Structural overlay of MpaG′ and LepI revealed a similar overall fold of the catalytic domain and also analogous binding mode of the cofactor SAH (Figure 6a). The *N*-terminal domain and the helical subdomain show more structural variations than the Rossman fold subdomain, consistent with the different sequence identities of these domains in the sequence alignment (Figure S6). The most significant difference

TABLE 1 Steady-state kinetic parameters of the three substrates.

Substrate	k_{cat} (min^{-1})	K_m (μM)	k_{cat}/K_m (min^{-1} $μM^{-1}$)
$MpaG'_{WT}$			
DMMPA	36.6 ± 1.4	39.4 ± 5.2	0.9
FDHMP-3C	39.8 ± 1.2	14.6 ± 1.9	2.7
FDHMP	37.8 ± 2.5	58.2 ± 12.7	0.7
$MpaG'_{Q267A}$			
DMMPA	36.9 ± 2.8	31.3 ± 8.9	1.2
FDHMP-3C	45.6 ± 1.6	11.5 ± 2.1	4.0
FDHMP	46.9 ± 2.1	29.9 ± 5.1	1.5

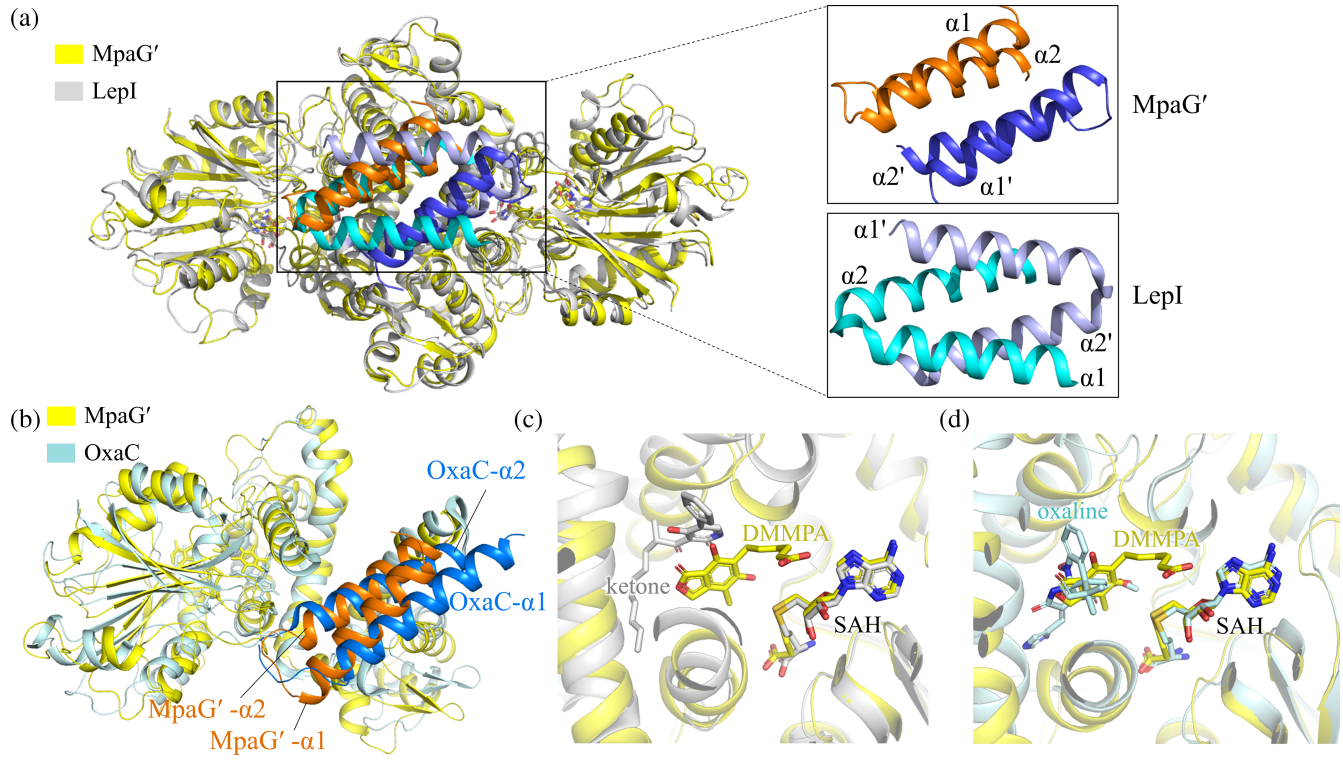

FIGURE 6 Structural comparison of MpaG′ with other homolog proteins. (a) Structural alignment of MpaG′ and the *O*-methyltransferase-like pericyclase LepI (PDB code: 6IX7). MpaG′ is colored in yellow with helices α1 and α2 shown in orange and blue in the two monomers. LepI is shown in gray with helices α1 and α2 colored in cyan and light blue in the two monomers. (b) Structural alignment of MpaG′ and classical OMT OxaC (PDB code: 5W7R). MpaG′ is displayed in the yellow cartoon with helices α1 and α2 highlighted in orange. OxaC is displayed in cyan with helices α1 and α2 highlighted in marine. (c) Structural comparison of the substrate binding pockets from MpaG′/SAH/DMMPA (yellow) and LepI/SAH/ketone (gray). (d) Structural alignment of the substrate binding pockets from MpaG′/SAH/DMMPA (yellow) and OxaC/SAH/oxaline (pale cyan).

lies in the *N*-terminal domain, in which MpaG′ harbors a four-helix bundle, but it is almost in parallel instead of interlocking like LepI (Figure 6a). The dimeric state of LepI was reported to be essential for its enzymatic activity and each homodimer was considered as a minimal integral functional unit (Cai et al., 2019; Sun et al., 2019). Another homolog of MpaG′ retrieved by the Dali server was a classical *O*-methyltransferase OxaC that methylates meleagrin to oxaline (PDB code: 5W7R) (Newmister et al., 2018), which has an RMSD of 3.1 Å with MpaG′ and exhibits a similar architecture of the 4-helix bundle (Figure 6b). However, the role of this bundle in OxaC remains unknown as deletion of the *N*-terminal two helices resulted in insolubility of OxaC (Newmister et al., 2018). To explore the role of the *N*-terminal helix bundle in typical *O*-methyltransferases, we performed in vitro enzymatic assays of a MpaG′ mutant with α1 and α2 double deletion. It was found that

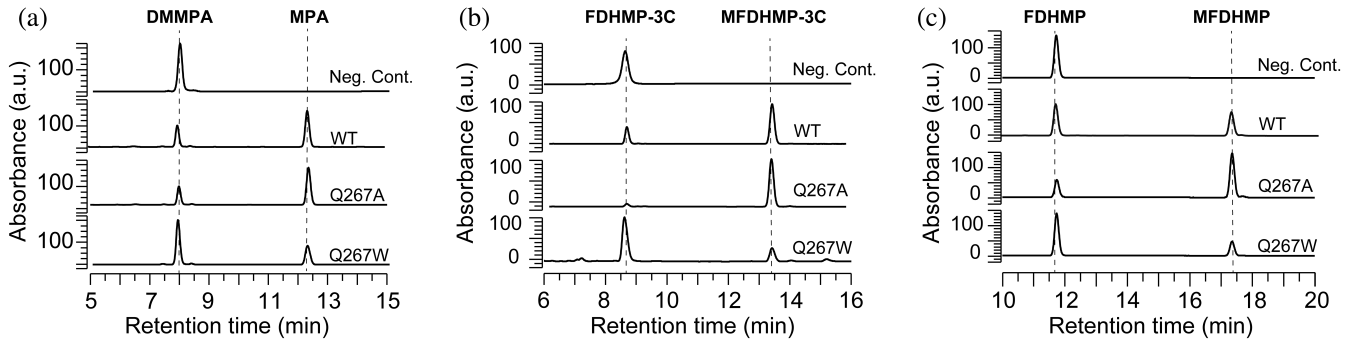

FIGURE 7 HPLC analysis (254 nm) of the enzymatic reactions catalyzed by the wild type (WT) and mutant MpaG′ enzymes using DMMPA (a), FDHMP-3C (b), and FDHMP (c) as substrates. The analytical scale reactions containing 1 μM MpaG′ (wild type or mutant), 5 mM SAM, and 0.5 mM substrate in 100 μl storage buffer were incubated at 40°C for 1 h.

the removal of α1 and α2 (Δα1-α2) led to a nearly complete loss of methylation activity towards FDHMP-3C, DMMPA, and FDHMP (Figure 3). These results indicate the critical role of α1 and α2 segments in the dimers for enzymatic activities of MpaG′.

Furthermore, although the helical subdomains of these structure homologs have similar organization of helices, the helical orientations and positions show variations for the accommodation of different substrates. LepI has evolved to be a pericyclase instead of a methyltransferase, so its substrate binding site on the helical subdomain is farther away from the SAM binding site (Figure 6c). The methyl receptor binding site of OxaC is close to the SAM binding site, similar to that observed in MpaG′, but the shapes of the substrate binding cavities of MpaG′ and OxaC are very different from each other because of their distinct substrate preference (Figure 6d).

3.7 | Semi-rational engineering of MpaG′

A more active MpaG′ mutant could enhance the synthetic efficiency of MPA, thus holding industrial application potential. To engineer such a mutant, by carefully analyzing the three different complex structures, we speculated that the salt bridge between R265 and the carboxyl tail of DMMPA or FDHMP-3C and other hydrophobic interactions could be sufficient for maintaining the right orientation of substrates. The residue Q267 with a long side chain at the substrate entrance channel may impede the entry of substrates. Thus, we semi-rationally mutated Q267 into an alanine, aiming to make a more accessible substrate entrance channel.

As expected, MpaG′$_{Q267A}$ exhibited 20% and 73% increase in substrate conversion ratios for FDHMP-3C and FDHMP, respectively, when compared to the wild-type MpaG′ (Figure 7). In addition to opening up the substrate entrance, the smaller side chain of alanine might also allow better accommodation of the long tails of FDHMP-3C and FDHMP (Figure 5b). By contrast, MpaG′$_{Q267A}$ only showed a slightly enhanced methylation activity towards DMMPA (73.5 ± 1.4% conversion) relative to MpaG′$_{WT}$ (67.9 ± 2.7% conversion), perhaps because the 267th amino acid residue has no contact with the shorter tail of DMMPA (Figure 5b). When Q267 was mutated to a tryptophan with a bulkier side chain, MpaG′$_{Q267W}$ lost a majority of its activity against the three substrates (Figure 7).

Furthermore, we conducted steady-state kinetic analyses for MpaG′$_{Q267A}$ (Table 1 and Figure S10b). Compared to MpaG′$_{WT}$, MpaG′$_{Q267A}$ demonstrated higher catalytic efficiencies (k_{cat}/K_m) towards DMMPA, FDHMP-3C and FDHMP to different extent. The improved catalytic efficiencies were unanimously due to increased k_{cat} and reduced K_m values. Thus, the kinetic results are well aligned with the proposed rationale and enzymatic activity measurements (Figure 7).

4 | DISCUSSION

MpaG′ is capable of catalyzing the 5-*O*-methylation of multiple intermediates in the mycophenolic acid biosynthetic pathway. This substrate flexibility is unusual for a biosynthetic methyltransferase, which normally shows high substrate specificity in order to maximally direct the metabolic flux to the final product (e.g., TylE/TylF (Bernard et al., 2015) and MycE/MycF (Li et al., 2009)). Aiming to elucidate the molecular basis for the catalytic mechanism and substrate flexibility of MpaG′, in this study, we resolved the crystal structures of MpaG′/SAH/DMMPA, MpaG′/SAH/FDHMP-3C and MpaG′/SAH/FDHMP. The structural and biochemical analyses confirmed H306-E362 to be the His-Glu catalytic dyad. Mechanistically, MpaG′ utilizes E362 to activate histidine H306, which then acts as a general base to deprotonate

the substrate nucleophile, namely the C5 hydroxyl group (Figure S9).

With regard to the substrate flexibility, the phthalide moiety shared by the three substrates (i.e., DMMPA, FDHMP-3C, and FDHMP) adopts almost identical conformation in the deep binding pocket in the three complex structures. The varying tail structures are located in the semi-open cavity which provides the flexibility to accommodate the differently tailored substrates. These tail structures form different hydrophobic and polar interactions with R265, Q267, V187, and P183, resulting in different binding affinities and catalytic efficiency towards DMMPA, FDHMP-3C, and FDHMP. Collectively, the phthalide moiety is the key component for substrate recognition and catalysis of MpaG′, while the length of the side chains is not crucial as long as they can enter the semi-open pocket, providing the substrate versatility with the significant expanding potential of MpaG′. By strategically modifying the chemical structures of native substrates, MpaG′ could be directed to produce novel products with potential pharmaceutical and bioactive applications. Furthermore, the unusual substrate flexibility of MpaG′ is a key factor in the MPA biosynthetic pathway, demonstrating the important impact that an individual tailoring enzyme can have on the profile of metabolites.

Homologous MpaG′ and LepI are both enzymes involved in fungal natural product biosynthesis. The non-methyltransferase functionality of LepI is a striking contrast to the normal methylation activity of MpaG′, especially considering that LepI evolved from a simple methyltransferase (Cai et al., 2019; Zhang et al., 2015). The structural comparison indicates that MpaG′ and LepI have similar catalytic domains and binding modes of the cofactor (Figure 6a, c). However, the sequence and structure similarity is not translated into functional similarity, which is evident by the fact that LepI catalyzes stereoselective dehydration and a number of pericyclic reactions, including intramolecular Diels-Alder and *hetero*-Diels-Alder cyclizations, rather than methylation. Thus, MpaG′ may also hold the potential to be engineered into a multifunctional enzyme for biotechnological applications.

In summary, we determined the crystal structures of the methyltransferase MpaG′ in the MPA biosynthetic pathway, including MpaG′/SAH/DMMPA, MpaG′/SAH/FDHMP-3C, and MpaG′/SAH/FDHMP complexes. The structures revealed that MpaG′ is an *O*-methyltransferase with a classical catalytic mechanism and innate substrate flexibility. The flexibility is originated from the semi-open substrate binding site which can accommodate different tail structures. The structural analysis provided the basis for the semi-rational engineering of MpaG′, which was exemplified by a $MpaG'_{Q267A}$ mutant with enhanced activity towards FDHMP-3C and FDHMP. The comparison of MpaG′ and its structural homologs suggests that *O*-methyltransferases have great potential to be engineered or designed to methylate diverse substrates. Therefore, this study provides not only a better understanding and new enhancing strategy of MPA biosynthesis but also important insights into the design and engineering of *O*-methyltransferases for structural diversification of natural products.

AUTHOR CONTRIBUTIONS

Cai You: Conceptualization; investigation; funding acquisition; writing – original draft; writing – review and editing. **Yunjun Pan:** Investigation; conceptualization; writing – original draft; funding acquisition; writing – review and editing. **Ruxin Liu:** Investigation. **Shengying Li:** Conceptualization; supervision; funding acquisition; writing – review and editing; investigation. **Yingang Feng:** Conceptualization; funding acquisition; writing – review and editing; supervision; investigation.

ACKNOWLEDGMENTS

This study was supported by the National Key Research and Development Program of China (2023YFC3402300 to Yingang Feng), the State Key Laboratory of Microbial Technology Open Projects Fund (M2022-01 to Yingang Feng), the National Natural Science Foundation of China (22237004 to Shengying Li, 32200030 to Cai You, 32070125 to Yingang Feng), QIBEBT (QIBEBT/SEI/QNESL S202302 to Yingang Feng), the China National Postdoctoral Program for Innovative Talents (BX20240210 to Yunjun Pan), the China Postdoctoral Science Foundation (2023M742087 to Yunjun Pan). We thank the staffs at BL02U1 and BL19U1 beamlines of the Shanghai Synchrotron Radiation Facility (SSRF) of the National Facility for Protein Science in Shanghai (NFPS), Shanghai Advanced Research Institute, Chinese Academy of Sciences, for X-ray diffraction data collection. We also thank Jingyao Qu, Jing Zhu, and Zhifeng Li from the State Key Laboratory of Microbial Technology of Shandong University for their help and guidance in LC–MS and NMR.

CONFLICT OF INTEREST STATEMENT

The authors declare no conflict of interest.

DATA AVAILABILITY STATEMENT

The structural coordinates of the SAH/DMMPA-MpaG′ complex, the SAH/FDHMP-3C-MpaG′ complex, and the SAH/FDHMP-MpaG′ complex have been deposited in the Protein Data Bank (PDB) under accession codes 8XTG, 8XTF, and 8XTE, respectively. The raw diffraction image data have been deposited in the SBGrid Data bank

(https://data.sbgrid.org) under dataset numbers 1100, 1102, and 1101.

ORCID

Shengying Li https://orcid.org/0000-0002-5244-870X
Yingang Feng https://orcid.org/0000-0002-0879-1316

REFERENCES

Adams PD, Afonine PV, Bunkóczi G, Chen VB, Davis IW, Echols N, et al. PHENIX: a comprehensive python-based system for macromolecular structure solution. Acta Crystallogr D Biol Crystallogr. 2010;66:213–21.

Bentley R. Mycophenolic acid: a one hundred year odyssey from antibiotic to immunosuppressant. Chem Rev. 2000;100:3801–25.

Bernard SM, Akey DL, Tripathi A, Park SR, Konwerski JR, Anzai Y, et al. Structural basis of substrate specificity and regiochemistry in the MycF/TylF family of sugar O-methyltransferases. ACS Chem Biol. 2015;10:1340–51.

Cai YJ, Hai Y, Ohashi M, Jamieson CS, Garcia-Borras M, Houk KN, et al. Structural basis for stereoselective dehydration and hydrogen-bonding catalysis by the SAM-dependent pericyclase Lepl. Nat Chem. 2019;11:812–20.

Cullen D, Leong SA, Wilson LJ, Henner DJ. Transformation of *Aspergillus nidulans* with the hygromycin-resistance gene, *hph*. Gene. 1987;57:21–6.

Du L, Li SY. Compartmentalized biosynthesis of fungal natural products. Curr Opin Biotechnol. 2021;69:128–35.

Emsley P, Lohkamp B, Scott WG, Cowtan K. Features and development of Coot. Acta Crystallogr D Biol Crystallogr. 2010;66:486–501.

Holm L, Rosenström P. Dali server: conservation mapping in 3D. Nucleic Acids Res. 2010;38:W545–9.

Joshi CP, Chiang VL. Conserved sequence motifs in plant *S*-adenosyl-L-methionine-dependent methyltransferases. Plant Mol Biol. 1998;37:663–74.

Jumper J, Evans R, Pritzel A, Green T, Figurnov M, Ronneberger O, et al. Highly accurate protein structure prediction with AlphaFold. Nature. 2021;596:583–9.

Kabsch W. XDS. Acta Crystallogr D Biol Crystallogr. 2010;66:125–32.

Knox HL, Sinner EK, Townsend CA, Boal AK, Booker SJ. Structure of a B_{12}-dependent radical SAM enzyme in carbapenem biosynthesis. Nature. 2022;602:343–8.

Kourounakis AP, Xanthopoulos D, Tzara A. Morpholine as a privileged structure: a review on the medicinal chemistry and pharmacological activity of morpholine containing bioactive molecules. Med Res Rev. 2020;40:709–52.

Krissinel E, Henrick K. Inference of macromolecular assemblies from crystalline state. J Mol Biol. 2007;372:774–97.

Lee Y-H, Ren D, Jeon B, Liu H-w. *S*-adenosylmethionine: more than just a methyl donor. Nat Prod Rep. 2023;40:1521–49.

Li JJ, Sun CX, Cai WN, Li J, Rosen BP, Chen J. Insights into *S*-adenosyl-L-methionine (SAM)-dependent methyltransferase related diseases and genetic polymorphisms. Mutat Res Rev Mutat Res. 2021;788:108396.

Li SY, Anzai Y, Kinoshita K, Kato F, Sherman DH. Functional analysis of MycE and MycF, two *O*-methyltransferases involved in the biosynthesis of mycinamicin macrolide antibiotics. Chembiochem. 2009;10:1297–301.

Liao L, Zhou Y, Peng T, Guo Y, Zhao Y, Zeng Z. Crystal structure of a *S*-adenosyl-L-methionine-dependent *O*-methyltransferase-like enzyme from *Aspergillus flavus*. Proteins. 2020;89:185–92.

Lin Z, Hu ZW, Zhou LJ, Liu BB, Huang XW, Deng ZX, et al. A large conserved family of small-molecule carboxyl methyltransferases identified from microorganisms. Proc Natl Acad Sci U S A. 2023;120:e2301389120.

Liscombe DK, Louie GV, Noel JP. Architectures, mechanisms and molecular evolution of natural product methyltransferases. Nat Prod Rep. 2012;29:1238–50.

McCoy AJ, Grosse-Kunstleve RW, Adams PD, Winn MD, Storoni LC, Read RJ. Phaser crystallographic software. J Appl Cryst. 2007;40:658–74.

Mitsui A, Suzuki S. Immunosuppressive effect of mycophenolic acid. J Antibiot. 1969;22:358–63.

Muth WL, Nash CH. Biosynthesis of mycophenolic acid: purification and characterization of S-adenosyl-L-methionine: demethylmycophenolic acid O-methyltransferase. Antimicrob Agents Chemother. 1975;8:321–7.

Newmister SA, Romminger S, Schmidt JJ, Williams RM, Smith JL, Berlinck RGS, et al. Unveiling sequential late-stage methyltransferase reactions in the meleagrin/oxaline biosynthetic pathway. Org Biomol Chem. 2018;16:6450–9.

Pan YJ, Gao LW, Zhang XJ, Qin YQ, Liu GD, Qu YB. The role of cross-pathway control regulator CpcA in the growth and extracellular enzyme production of *Penicillium oxalicum*. Curr Microbiol. 2020;77:49–54.

Planterose DN. Antiviral and cytotoxic effects of mycophenolic acid. J Gen Virol. 1969;4:629–30.

Scharf DH, Habel A, Heinekamp T, Brakhage AA, Hertweck C. Opposed effects of enzymatic gliotoxin *N*- and *S*-methylations. J Am Chem Soc. 2014;136:11674–9.

Schubert HL, Blumenthal RM, Cheng XD. Many paths to methyltransfer: a chronicle of convergence. Trends Biochem Sci. 2003;28:329–35.

Subrizi F, Wang Y, Thair B, Méndez-Sánchez D, Roddan R, Cárdenas-Fernández M, et al. Multienzyme one-pot cascades incorporating methyltransferases for the strategic diversification of tetrahydroisoquinoline alkaloids. Angew Chem Int Edit. 2021;60:18673–9.

Sun Q, Hu YH, Gu YJ, Huang JK, He J, Luo L, et al. Deciphering the regulatory and catalytic mechanisms of an unusual SAM-dependent enzyme. Signal Transduct Target Ther. 2019;4:17.

Vaishnav P, Demain AL. Unexpected applications of secondary metabolites. Biotechnol Adv. 2011;29:223–9.

Wang Q-S, Zhang K-H, Cui Y, Wang Z-J, Pan Q-Y, Liu K, et al. Upgrade of macromolecular crystallography beamline BL17U1 at SSRF. Nucl Sci Tech. 2018;29:68.

Williams CJ, Headd JJ, Moriarty NW, Prisant MG, Videau LL, Deis LN, et al. MolProbity: more and better reference data for improved all-atom structure validation. Protein Sci. 2018;27:293–315.

Yang Y, Yuan JS, Ross J, Noel JP, Pichersky E, Chen F. An *Arabidopsis thaliana* methyltransferase capable of methylating farnesoic acid. Arch Biochem Biophys. 2006;448:123–32.

You C, Li FW, Zhang XW, Ma L, Zhang YZ, Zhang W, et al. Structural basis for substrate specificity of the peroxisomal acyl-CoA

hydrolase MpaH' involved in mycophenolic acid biosynthesis. FEBS J. 2021;288:5768–80.

Yu JH, Hamari Z, Han KH, Seo JA, Reyes-Domínguez Y, Scazzocchio C. Double-joint PCR: a PCR-based molecular tool for gene manipulations in filamentous fungi. Fungal Genet Biol. 2004;41:973–81.

Zhang J, Zheng YG. SAM/SAH analogs as versatile tools for SAM-dependent methyltransferases. ACS Chem Biol. 2016;11:583–97.

Zhang W, Cao SN, Qiu L, Qi FX, Li Z, Yang Y, et al. Functional characterization of MpaG', the *O*-methyltransferase involved in the biosynthesis of mycophenolic acid. Chembiochem. 2015;16:565–9.

Zhang W, Du L, Qu ZP, Zhang XW, Li FW, Li Z, et al. Compartmentalized biosynthesis of mycophenolic acid. Proc Natl Acad Sci USA. 2019;116:13305–10.

Zhang W-Z, Tang J-C, Wang S-S, Wang Z-J, Qin W-M, He J-H. The protein complex crystallography beamline (BL19U1) at the Shanghai synchrotron radiation facility. Nucl Sci Tech. 2019;30:170.

Zubieta C, He XZ, Dixon RA, Noel JP. Structures of two natural product methyltransferases reveal the basis for substrate specificity in plant *O*-methyltransferases. Nat Struct Biol. 2001;8:271–9.

SUPPORTING INFORMATION

Additional supporting information can be found online in the Supporting Information section at the end of this article.

How to cite this article: You C, Pan Y, Liu R, Li S, Feng Y. Structural basis for substrate flexibility of the *O*-methyltransferase MpaG' involved in mycophenolic acid biosynthesis. Protein Science. 2024;33(9):e5144. https://doi.org/10.1002/pro.5144